Acta Mech 229, 403–420 (2018)
https://doi.org/10.1007/s00707-017-1978-1

ORIGINAL PAPER

S. Sahmani · M. M. Aghdam

Nonlinear instability of hydrostatic pressurized microtubules surrounded by cytoplasm of a living cell including nonlocality and strain gradient microsize dependency

Received: 8 June 2017 / Revised: 24 August 2017 / Published online: 6 October 2017

Abstract As one of the most important components of a cytoskeleton, microtubules made from tubular polymers of tubulin can be found throughout the cytoplasm of eukaryotic cells. The role of microtubules in maintaining the structures of a living cell under external mechanical load is essential, so it is necessary to anticipate their size-dependent mechanical characteristics. In the present study, the size-dependent nonlinear instability of microtubules embedded in the biomedium of a living cell and under hydrostatic pressure is analyzed at different temperatures. For this objective, a more comprehensive size-dependent elasticity theory such as nonlocal strain gradient theory of elasticity is implemented to a refined hyperbolic shear deformation shell theory. Through deduction of the nonclassical governing equations to boundary layer-type ones and then employing a two-stepped perturbation solving process, explicit analytical expressions are established for nonlocal strain gradient stability paths of hydrostatic pressurized microtubules surrounded by the cytoplasm of a living cell. It is observed that for a microtubule under hydrostatic pressure, an initial extension occurs in the prebuckling regime until the critical buckling pressure. The nonlocality size effect decreases this initial extension, but the strain gradient size dependency increases it.

1 Introduction

A microtubule made from a single type of globular protein can be considered as a filamentous intracellular structure which makes up the internal shape of cilia and flagella in a living eukaryotic cell. Moreover, it plays an essential role in a variety of cellular processes. As a result, it is important to accurately capture the size dependency in the mechanical behavior of microtubules. A few experimental investigations have been carried out in laboratories to evaluate the elastic properties as well as mechanical characteristics of microtubules under different loading conditions [1–4], but because of the scattering of presented experimental results over a wide range, their consistency is not reliable.

Modeling of a nanosized material as a continuum object rather than as discrete material incorporating size effects is another way to deal with predicting the mechanical responses of nanostructures efficiently. To this end, several nonclassical continuum theories of elasticity have been proposed and put to use in order to analyze the size-dependent behavior of structures at nanoscale [5–29]. These theories have also been employed to analyze the size effects in the mechanical behavior of microtubules. For instance, Shen [30] analyzed the axial buckling and postbuckling behavior of microtubules embedded in an elastic medium on the basis of nonlocal continuum theory. Li et al. [31] investigated the influence of bioliquid density and biomedium on the coupling frequency of bioliquid-filled microtubules based on nonlocal elasticity theory. Daneshmand et al.

S. Sahmani (✉) · M. M. Aghdam
Department of Mechanical Engineering, Amirkabir University of Technology, P.O. Box 15875-4413, Tehran, Iran
E-mail: sahmani@aut.ac.ir
Tel.: +98 21 66405844
Fax: +98 21 66419736

[32] used nonlocal elasticity theory within the framework of higher-order shear deformation shell theory to predict the wave propagation of microtubules. Wang et al. [33] reported an analytical method on the basis of nonlocal continuum elasticity to analyze the influence of initial stress on the dynamic response of bioliquid-filled microtubules. Based upon couple stress elasticity theory in conjunction with surface elasticity theory, Ghorbanpour Arani et al. [34] studied the free vibration behavior of bioliquid-filled microtubules. Civalek and Demir [35] introduced a simple nonlocal Euler–Bernoulli beam model for the buckling analysis of a protein microtubule using the finite element method. Sahmani and Aghdam [36] studied the nonlinear postbuckling behavior of an axially loaded microtubule surrounded by the cytoplasm biomedium based on a nonlocal strain gradient shell model.

Generally, in the previous investigations, it has been observed that the size effect in type of stress nonlocality has a softening influence, while the strain gradient size dependency leads to a stiffening effect. Accordingly, Lim et al. [37] proposed a more comprehensive size-dependent elasticity theory such as nonlocal strain gradient theory which includes both the softening and stiffening influences to describe the size dependency in a more accurate way. Afterward, a few studies have been performed on the basis of nonlocal strain gradient elasticity theory. Li et al. [38] presented the longitudinal vibration analysis of nanorods based on nonlocal strain gradient continuum theory. Yang et al. [39] incorporated jointly the nonlocal stress and strain gradients to obtain the size-dependent dynamic pull-in voltages of nanoscaled actuators. Li and Hu [40] developed a size-dependent Euler–Bernoulli beam model on the basis of nonlocal strain gradient elasticity theory for nonlinear buckling analysis of nanobeams. Tang et al. [41] proposed a nonlocal strain gradient beam model to study the viscoelastic wave propagation in embedded single-walled carbon nanotubes. Ebrahimi and Barati [42] evaluated the hygrothermal effects on damping vibration behavior of functionally graded viscoelastic nanobeams via nonlocal strain gradient theory of elasticity. Sahmani and Aghdam [43] constructed a nonlocal strain gradient beam model for the size-dependent nonlinear vibration response of a postbuckled multilayer functionally graded nanobeam. Li and Hu [44] employed the nonlocal strain gradient elasticity theory within the framework of the Euler–Bernoulli beam theory to analyze the postbuckling behavior of functionally graded nanobeams. Zhu and Li [45] presented a closed-form solution for a small-scaled rod in tension on the basis of the nonlocal strain gradient theory of elasticity.

In the current work, the nonlocal strain gradient continuum theory of elasticity is implemented for the first time in a refined hyperbolic shear deformation shell theory to anticipate the temperature-dependent nonlinear instability of hydrostatic pressurized microtubules embedded in a cytoplasm biomedium including simultaneously both the stiffening and softening small-scale effects. The size-dependent stability curves are obtained corresponding to various values of nonlocal and internal strain gradient length scale parameters and different temperatures.

2 Nonlocal strain gradient orthotropic shell model

In Fig. 1, it is depicted that a microtubule made from a functional subunit such as heterodimer proteins which contain α and β tubulin bounding spontaneously one another is assumed as a cylindrical nanoshell with the length, outer radius, inner radius and effective thickness of L, R_o, R_i and h, respectively. In this investigation, a microtubule with 3 numbers of start and 13 numbers of protofilament is considered in order to make related skew angle equal to zero. As a result, the microtubule can be modeled via an orthotropic shell with inner diameter of 17.4 nm and outer diameter of 25.4 nm which results in the mean radius of $R = 10.7$ nm. Also, the effective shell thickness is estimated as $h = 1.6$ nm.

Within the framework of hyperbolic shear deformation theory [46], the displacement field related to cylindrical shell can be given as

$$u_x(x, y, z) = u(x, y) - z\frac{\partial w(x, y)}{\partial x} + \left(z\cosh\left(\frac{1}{2}\right) - h\sinh\left(\frac{z}{h}\right)\right)\psi_x(x, y), \tag{1a}$$

$$u_y(x, y, z) = v(x, y) - z\frac{\partial w(x, y)}{\partial y} + \left(z\cosh\left(\frac{1}{2}\right) - h\sinh\left(\frac{z}{h}\right)\right)\psi_y(x, y), \tag{1b}$$

$$u_z(x, y, z) = w(x, y), \tag{1c}$$

where u, v and w in order are the axial, circumferential and transverse displacements of microtubule. Also, ψ_x and ψ_y are, respectively, the rotations of the cross section of microtubule at the neutral plane normal about the y- and x-axis.

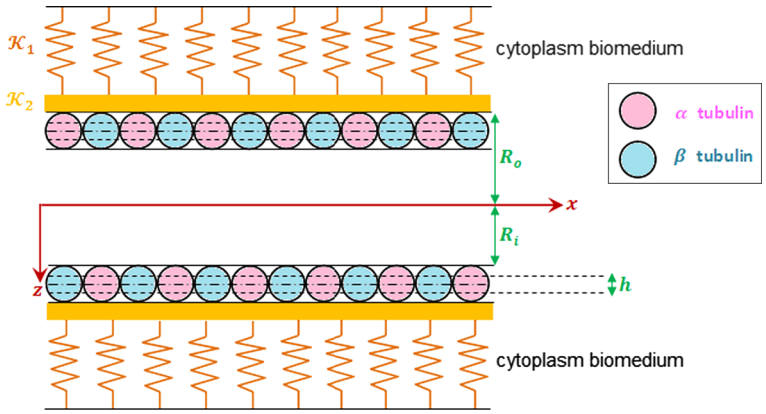

Fig. 1 Schematic representation of a microtubule embedded in cytoplasm biomedium

According to the von Karman–Donnell type of nonlinearity kinematics [47], the strain–displacement relationships can be expressed as

$$\begin{aligned}
&\left\{\begin{matrix}\varepsilon_{xx}\\ \varepsilon_{yy}\\ \gamma_{xy}\end{matrix}\right\}+\left\{\begin{matrix}\varepsilon^T_{xx}\\ \varepsilon^T_{yy}\\ \gamma^T_{xy}\end{matrix}\right\}=\left\{\begin{matrix}\varepsilon^0_{xx}\\ \varepsilon^0_{yy}\\ \gamma^0_{xy}\end{matrix}\right\}+\left\{\begin{matrix}\varepsilon^T_{xx}\\ \varepsilon^T_{yy}\\ \gamma^T_{xy}\end{matrix}\right\}+z\left\{\begin{matrix}\kappa^{(1)}_{xx}\\ \kappa^{(1)}_{yy}\\ \kappa^{(1)}_{xy}\end{matrix}\right\}+\left(z\cosh\left(\frac{1}{2}\right)-h\sinh\left(\frac{z}{h}\right)\right)\left\{\begin{matrix}\kappa^{(2)}_{xx}\\ \kappa^{(2)}_{yy}\\ \kappa^{(2)}_{xy}\end{matrix}\right\}\\
&=\left\{\begin{matrix}\frac{\partial u}{\partial x}+\frac{1}{2}\left(\frac{\partial w}{\partial y}\right)^2\\ \frac{\partial v}{\partial y}-\frac{w}{R}+\frac{1}{2}\left(\frac{\partial w}{\partial y}\right)^2\\ \frac{\partial u}{\partial y}+\frac{\partial v}{\partial x}+\frac{\partial w}{\partial x}\frac{\partial w}{\partial y}\end{matrix}\right\}+\left\{\begin{matrix}\alpha_{11}\Delta T\\ \alpha_{22}\Delta T\\ 0\end{matrix}\right\}-z\left\{\begin{matrix}\frac{\partial^2 w}{\partial x^2}\\ \frac{\partial^2 w}{\partial y^2}\\ 2\frac{\partial^2 w}{\partial x\partial y}\end{matrix}\right\}\\
&+\left(z\cosh\left(\frac{1}{2}\right)-h\sinh\left(\frac{z}{h}\right)\right)\left\{\begin{matrix}\frac{\partial\psi_x}{\partial x}\\ \frac{\partial\psi_y}{\partial y}\\ \frac{\partial\psi_x}{\partial y}+\frac{\partial\psi_y}{\partial x}\end{matrix}\right\}\\
&\left\{\begin{matrix}\gamma_{xz}\\ \gamma_{yz}\end{matrix}\right\}=\left(\cosh\left(\frac{1}{2}\right)-\cosh\left(\frac{z}{h}\right)\right)\left\{\begin{matrix}\psi_x\\ \psi_y\end{matrix}\right\}
\end{aligned}\tag{2}$$

in which $\varepsilon^0_{ij}, \varepsilon^T_{ij}, \kappa^{(1)}_{ij}, \kappa^{(2)}_{ij}$ $(i, j = x, y)$ represent, respectively, the mid-plane strain components, thermal strain components, the first-order curvature components and the higher-order curvature components. Additionally, α_{11}, α_{22} are thermal expansion coefficients of the microtubule, and ΔT denotes the temperature change from room temperature (30 °C).

As was mentioned before, it has been observed that small-scale effects may cause a softening or stiffening influence. Motivated by this fact, Lim et al. [37] proposed a new unconventional continuum theory, the nonlocal strain gradient elasticity theory, which contains the both nonlocal and strain gradient size effects simultaneously. As a result, the total nonlocal strain gradient stress tensor Λ can be expressed as [37]

$$\Lambda_{ij} = \sigma_{ij} - \nabla\sigma^*_{ij}; \quad i, j = x, y, \tag{3}$$

where σ and σ^* in order denote the stress and higher-order stress tensors which can be defined as

$$\sigma_{ij} = \int_\Omega \left\{\varrho_1(|\mathcal{X}' - \mathcal{X}|)C_{ijkl}\varepsilon_{kl}(\mathcal{X}')\right\} d\Omega, \tag{4a}$$

$$\sigma_{ij} = l^2\int_\Omega \left\{\varrho_2(|\mathcal{X}' - \mathcal{X}|)C_{ijkl}\nabla\varepsilon_{kl}(\mathcal{X}')\right\} d\Omega, \tag{4b}$$

in which C is the stiffness matrix, ϱ_1 and ϱ_2 are, respectively, the principal attenuation kernel function including the nonlocality and the additional kernel function associated with the nonlocality effect of the first-order strain

gradient field, $\mathcal{X}$ and $\mathcal{X}'$ in order represent a point and any point else in the body, and l stands for the internal length scale parameter. Also, ∇ is the gradient symbol. Following the method of Eringen, the constitutive relationship corresponding to the total nonlocal strain gradient stress tensor of a two-dimensional material can be obtained as

$$\left(1-e_0^2\theta^2\nabla^2\right)\Lambda_{ij}=C_{ijkl}\varepsilon_{kl}-l^2C_{ijkl}\nabla^2\varepsilon_{kl}, \tag{5}$$

where $e_0\theta$ represents the nonlocal parameter in such a way that θ is an internal characteristic constant and e_0 is a constant related to the selected material. In addition, ∇^2 denotes the Laplacian operator. As a result, the nonlocal strain gradient constitutive relations for a microtubule can be rewritten as

$$\begin{aligned}
&\left(1-e_0^2\theta^2\nabla^2\right)\begin{Bmatrix}\sigma_{xx}\\ \sigma_{yy}\\ \sigma_{yz}\\ \sigma_{xz}\\ \sigma_{xy}\end{Bmatrix}\\
&=\left(1-l^2\nabla^2\right)\begin{bmatrix}Q_{11}&Q_{12}&0&0&0\\ Q_{12}&Q_{22}&0&0&0\\ 0&0&Q_{44}&0&0\\ 0&0&0&Q_{55}&0\\ 0&0&0&0&Q_{66}\end{bmatrix}\begin{Bmatrix}\varepsilon_{xx}\\ \varepsilon_{yy}\\ \gamma_{yz}\\ \gamma_{xz}\\ \gamma_{xy}\end{Bmatrix}\\
&+\begin{bmatrix}Q_{11}&Q_{12}&0&0&0\\ Q_{12}&Q_{22}&0&0&0\\ 0&0&Q_{44}&0&0\\ 0&0&0&Q_{55}&0\\ 0&0&0&0&Q_{66}\end{bmatrix}\begin{bmatrix}1&0\\ 0&1\\ 0&0\\ 0&0\\ 0&0\end{bmatrix}\begin{Bmatrix}\alpha_{11}\Delta T\\ \alpha_{22}\Delta T\end{Bmatrix},
\end{aligned} \tag{6}$$

in which the temperature-dependent stiffness parameters can be defined as

$$\begin{aligned}
&Q_{11}(T)=\frac{E_{11}(T)}{1-\nu_{12}\nu_{21}},\quad Q_{22}(T)=\frac{E_{22}(T)}{1-\nu_{12}\nu_{21}},\quad Q_{12}(T)=\frac{\nu_{12}E_{22}(T)}{1-\nu_{12}\nu_{21}},\\
&Q_{44}(T)=G_{23}(T),\quad Q_{55}(T)=G_{13}(T),\quad Q_{66}(T)=G_{12}(T).
\end{aligned} \tag{7}$$

The external work done by a cytoplasm type of biomedium elastic foundation can be expressed as

$$\Pi_P=\int_S\left(\mathcal{K}_1w^2+\mathcal{K}_2\left(\left(\frac{\partial w}{\partial x}\right)^2+\left(\frac{\partial w}{\partial y}\right)^2\right)\right)\mathrm{d}S, \tag{8}$$

in which $\mathcal{K}_1$ and $\mathcal{K}_2$ in order are the normal and shear stiffness of the cytoplasm type of biomedium elastic foundation, respectively.

In addition, the work Π_P done by the external hydrostatic pressure q can be expressed as

$$\Pi_P=\int_S qw\mathrm{d}S. \tag{9}$$

Based upon the nonlocal strain gradient orthotropic shell model, the total strain energy of a microtubule can be written as

$$\begin{aligned}
\Pi_s&=\frac{1}{2}\int_S\int_{-\frac{h}{2}}^{\frac{h}{2}}\left\{\sigma_{ij}\varepsilon_{ij}+\sigma_{ij}^*\nabla\varepsilon_{ij}\right\}\mathrm{d}z\mathrm{d}S\\
&=\frac{1}{2}\int_S\Big\{N_{xx}\varepsilon_{xx}^0+N_{yy}\varepsilon_{yy}^0+N_{xy}\gamma_{xy}^0+M_{xx}\kappa_{xx}^{(1)}+M_{yy}\kappa_{yy}^{(1)}+M_{xy}\kappa_{xy}^{(1)}+H_{xx}\kappa_{xx}^{(2)}+H_{yy}\kappa_{yy}^{(2)}\\
&\quad+H_{xy}\kappa_{xy}^{(2)}+Q_x\gamma_{xz}+Q_y\gamma_{yz}\Big\}\mathrm{d}S,
\end{aligned} \tag{10}$$

where the stress resultants are:

$$\left\{\begin{array}{l} N_{xx}-e_0^2\theta^2\nabla^2 N_{xx} \\ N_{yy}-e_0^2\theta^2\nabla^2 N_{yy} \\ N_{xy}-e_0^2\theta^2\nabla^2 N_{xy} \end{array}\right\} = \left[\begin{array}{ccc} A_{11}^* & A_{12}^* & 0 \\ A_{12}^* & A_{22}^* & 0 \\ 0 & 0 & A_{66}^* \end{array}\right] \left\{\begin{array}{l} \varepsilon_{xx}^0-l^2\nabla^2\varepsilon_{xx}^0 \\ \varepsilon_{yy}^0-l^2\nabla^2\varepsilon_{yy}^0 \\ \gamma_{xy}^0-l^2\nabla^2\gamma_{xy}^0 \end{array}\right\} - \left\{\begin{array}{l} N_{xx}^T \\ N_{yy}^T \\ 0 \end{array}\right\},$$

$$\left\{\begin{array}{l} M_{xx}-e_0^2\theta^2\nabla^2 M_{xx} \\ M_{yy}-e_0^2\theta^2\nabla^2 M_{xx} \\ M_{xy}-e_0^2\theta^2\nabla^2 M_{xx} \end{array}\right\} = \left[\begin{array}{ccc} D_{11}^* & D_{12}^* & 0 \\ D_{12}^* & D_{22}^* & 0 \\ 0 & 0 & D_{66}^* \end{array}\right] \left\{\begin{array}{l} \kappa_{xx}^{(1)}-l^2\nabla^2\kappa_{xx}^{(1)} \\ \kappa_{yy}^{(1)}-l^2\nabla^2\kappa_{yy}^{(1)} \\ \kappa_{xy}^{(1)}-l^2\nabla^2\kappa_{xy}^{(1)} \end{array}\right\} + \left[\begin{array}{ccc} D_{11}^{**} & D_{12}^{**} & 0 \\ D_{12}^{**} & D_{22}^{**} & 0 \\ 0 & 0 & D_{66}^{**} \end{array}\right] \left\{\begin{array}{l} \kappa_{xx}^{(2)}-l^2\nabla^2\kappa_{xx}^{(2)} \\ \kappa_{yy}^{(2)}-l^2\nabla^2\kappa_{yy}^{(2)} \\ \kappa_{xy}^{(2)}-l^2\nabla^2\kappa_{xy}^{(2)} \end{array}\right\},$$

$$\left\{\begin{array}{l} H_{xx}-e_0^2\theta^2\nabla^2 H_{xx} \\ H_{yy}-e_0^2\theta^2\nabla^2 H_{xx} \\ H_{xy}-e_0^2\theta^2\nabla^2 H_{xx} \end{array}\right\} = \left[\begin{array}{ccc} D_{11}^{**} & D_{12}^{**} & 0 \\ D_{12}^{**} & D_{22}^{**} & 0 \\ 0 & 0 & D_{66}^{**} \end{array}\right] \left\{\begin{array}{l} \kappa_{xx}^{(1)}-l^2\nabla^2\kappa_{xx}^{(1)} \\ \kappa_{yy}^{(1)}-l^2\nabla^2\kappa_{yy}^{(1)} \\ \kappa_{xy}^{(1)}-l^2\nabla^2\kappa_{xy}^{(1)} \end{array}\right\} + \left[\begin{array}{ccc} G_{11}^* & G_{12}^* & 0 \\ G_{12}^* & G_{22}^* & 0 \\ 0 & 0 & G_{66}^* \end{array}\right] \left\{\begin{array}{l} \kappa_{xx}^{(2)}-l^2\nabla^2\kappa_{xx}^{(2)} \\ \kappa_{yy}^{(2)}-l^2\nabla^2\kappa_{yy}^{(2)} \\ \kappa_{xy}^{(2)}-l^2\nabla^2\kappa_{xy}^{(2)} \end{array}\right\},$$

$$\left\{\begin{array}{l} Q_x-e_0^2\theta^2\nabla^2 Q_x \\ Q_y-e_0^2\theta^2\nabla^2 Q_y \end{array}\right\} = \left[\begin{array}{cc} A_{44}^* & 0 \\ 0 & A_{55}^* \end{array}\right] \left\{\begin{array}{l} \psi_x-l^2\nabla^2\psi_x \\ \psi_y-l^2\nabla^2\psi_y \end{array}\right\}, \tag{11}$$

in which

$$\left\{\begin{array}{l} N_{xx} \\ N_{yy} \\ N_{xy} \end{array}\right\} = \int_{-\frac{h}{2}}^{\frac{h}{2}} \left\{\begin{array}{l} \Lambda_{xx} \\ \Lambda_{yy} \\ \Lambda_{xy} \end{array}\right\} \mathrm{d}z, \quad \left\{\begin{array}{l} M_{xx} \\ M_{yy} \\ M_{xy} \end{array}\right\} = \int_{-\frac{h}{2}}^{\frac{h}{2}} \left\{\begin{array}{l} \Lambda_{xx} \\ \Lambda_{yy} \\ \Lambda_{xy} \end{array}\right\} z\mathrm{d}z, \quad \left\{\begin{array}{l} N_{xx}^T \\ N_{yy}^T \end{array}\right\} = \left\{\begin{array}{l} \left(A_{11}^*+A_{12}^*\right)\alpha_{11} \\ \left(A_{22}^*+A_{12}^*\right)\alpha_{22} \end{array}\right\} \Delta T,$$

$$\left\{\begin{array}{l} H_{xx} \\ H_{yy} \\ H_{xy} \end{array}\right\} = \int_{-\frac{h}{2}}^{\frac{h}{2}} \left\{\begin{array}{l} \Lambda_{xx} \\ \Lambda_{yy} \\ \Lambda_{xy} \end{array}\right\} \left(z\cosh\left(\frac{1}{2}\right) - h\sinh\left(\frac{z}{h}\right)\right) \mathrm{d}z,$$

$$\left\{\begin{array}{l} Q_x \\ Q_y \end{array}\right\} = \int_{-\frac{h}{2}}^{\frac{h}{2}} \left\{\begin{array}{l} \Lambda_{xz} \\ \Lambda_{yz} \end{array}\right\} \left(\cosh\left(\frac{1}{2}\right) - \cosh\left(\frac{z}{h}\right)\right) \mathrm{d}z \tag{12}$$

and

$$\left\{\begin{array}{l} A_{11}^*, D_{11}^* \\ D_{11}^{**}, G_{11}^* \end{array}\right\} = \int_{-h/2}^{h/2} [Q_{11}] \left\{\begin{array}{l} 1, z^2 \\ z^2\cosh\left(\frac{1}{2}\right) - zh\sinh\left(\frac{z}{h}\right), \left(z\cosh\left(\frac{1}{2}\right) - h\sinh\left(\frac{z}{h}\right)\right)^2 \end{array}\right\} \mathrm{d}z,$$

$$\left\{\begin{array}{l} A_{22}^*, D_{22}^* \\ D_{22}^{**}, G_{22}^* \end{array}\right\} = \int_{-h/2}^{h/2} [Q_{22}] \left\{\begin{array}{l} 1, z^2 \\ z^2\cosh\left(\frac{1}{2}\right) - zh\sinh\left(\frac{z}{h}\right), \left(z\cosh\left(\frac{1}{2}\right) - h\sinh\left(\frac{z}{h}\right)\right)^2 \end{array}\right\} \mathrm{d}z,$$

$$\left\{\begin{array}{l} A_{12}^*, D_{12}^* \\ D_{12}^{**}, G_{12}^* \end{array}\right\} = \int_{-h/2}^{h/2} [Q_{12}] \left\{\begin{array}{l} 1, z^2 \\ z^2\cosh\left(\frac{1}{2}\right) - zh\sinh\left(\frac{z}{h}\right), \left(z\cosh\left(\frac{1}{2}\right) - h\sinh\left(\frac{z}{h}\right)\right)^2 \end{array}\right\} \mathrm{d}z,$$

$$\left\{\begin{array}{l} A_{66}^*, D_{66}^* \\ D_{66}^{**}, G_{66}^* \end{array}\right\} = \int_{-h/2}^{h/2} [Q_{66}] \left\{\begin{array}{l} 1, z^2 \\ z^2\cosh\left(\frac{1}{2}\right) - zh\sinh\left(\frac{z}{h}\right), \left(z\cosh\left(\frac{1}{2}\right) - h\sinh\left(\frac{z}{h}\right)\right)^2 \end{array}\right\} \mathrm{d}z,$$

$$\left\{\begin{array}{l} A_{44}^* \\ A_{55}^* \end{array}\right\} = \left\{\begin{array}{l} \int_{-h/2}^{h/2} [Q_{44}] \left(\cosh\left(\frac{1}{2}\right) - \cosh\left(\frac{z}{h}\right)\right) \mathrm{d}z \\ \int_{-h/2}^{h/2} [Q_{55}] \left(\cosh\left(\frac{1}{2}\right) - \cosh\left(\frac{z}{h}\right)\right) \mathrm{d}z \end{array}\right\}. \tag{13}$$

By applying the virtual work's principle to the total strain energy of the microtubule modeled via the hyperbolic shear deformable orthotropic shell model, the nonclassical governing differential equations are

derived as

$$\frac{\partial N_{xx}}{\partial x}+\frac{\partial N_{xy}}{\partial y}=0, \tag{14a}$$

$$\frac{\partial N_{xy}}{\partial x}+\frac{\partial N_{yy}}{\partial y}=0, \tag{14b}$$

$$\frac{\partial^2 M_{xx}}{\partial x^2}+2\frac{\partial^2 M_{xy}}{\partial x\partial y}+\frac{\partial^2 M_{yy}}{\partial y^2}+\frac{N_{yy}}{R}+N_{xx}\frac{\partial^2 w}{\partial x^2}+2N_{xy}\frac{\partial^2 w}{\partial x\partial y}+N_{yy}\frac{\partial^2 w}{\partial y^2}-\mathcal{K}_1 w$$
$$+\mathcal{K}_2\left(\frac{\partial^2 w}{\partial x^2}+\frac{\partial^2 w}{\partial y^2}\right)+q=0, \tag{14c}$$

$$\frac{\partial H_{xx}}{\partial x}+\frac{\partial H_{xy}}{\partial y}-Q_x=0, \tag{14d}$$

$$\frac{\partial H_{xy}}{\partial x}+\frac{\partial H_{yy}}{\partial y}-Q_y=0. \tag{14e}$$

With the aim of satisfaction of the first two differential equations at hand, the Airy stress function $f\,(x,y)$ is introduced as

$$N_{xx}=\frac{\partial^2 f\,(x,y)}{\partial y^2},\quad N_{yy}=\frac{\partial^2 f\,(x,y)}{\partial x^2},\quad N_{xy}=-\frac{\partial^2 f\,(x,y)}{\partial x\partial y}. \tag{15}$$

Additionally, for a perfect shell-type structure, the compatibility equation relevant to the mid-plane strain components can be written as

$$\frac{\partial^2 \varepsilon^0_{xx}}{\partial y^2}+\frac{\partial^2 \varepsilon^0_{yy}}{\partial x^2}-\frac{\partial^2 \gamma^0_{xy}}{\partial x\partial y}=\left(\frac{\partial^2 w}{\partial x\partial y}\right)^2-\frac{\partial^2 w}{\partial x^2}\frac{\partial^2 w}{\partial y^2}-\frac{1}{R}\frac{\partial^2 w}{\partial x^2}. \tag{16}$$

Therefore, through inserting Eq. (15) in the inverse of Eq. (11) and then using Eqs. (14) and (16), the nonlocal strain gradient governing equations can be presented as functions of the displacement field as follows:

$$\left(\frac{A^*_{11}}{A^*_{11}A^*_{22}-\left(A^*_{12}\right)^2}\right)\frac{\partial^4 f}{\partial x^4}+\left(\frac{1}{A^*_{66}}-\frac{2A^*_{12}}{A^*_{11}A^*_{22}-\left(A^*_{12}\right)^2}\right)\frac{\partial^4 f}{\partial x^2\partial y^2}+\left(\frac{A^*_{22}}{A^*_{11}A^*_{22}-\left(A^*_{12}\right)^2}\right)\frac{\partial^4 f}{\partial y^4}+\frac{1}{R}\frac{\partial^2 w}{\partial x^2}$$
$$=\left(\frac{\partial^2 w}{\partial x\partial y}\right)^2-\frac{\partial^2 w}{\partial x^2}\frac{\partial^2 w}{\partial y^2}, \tag{17a}$$

$$\left(1-l^2\nabla^2\right)\left(D^*_{11}\frac{\partial^4 w}{\partial x^4}+2\left(D^*_{12}+2D^*_{66}\right)\frac{\partial^4 w}{\partial x^2\partial y^2}+D^*_{22}\frac{\partial^4 w}{\partial y^4}-D^{**}_{11}\frac{\partial^3 \psi_x}{\partial x^3}-\left(D^{**}_{12}+2D^{**}_{66}\right)\frac{\partial^3 \psi_x}{\partial x\partial y^2}\right.$$
$$\left.-D^{**}_{22}\frac{\partial^3 \psi_y}{\partial y^3}-\left(D^{**}_{12}+2D^{**}_{66}\right)\frac{\partial^3 \psi_y}{\partial x^2\partial y}\right)+\mathcal{K}_1 w-\mathcal{K}_2\left(\frac{\partial^2 w}{\partial x^2}+\frac{\partial^2 w}{\partial y^2}\right)$$
$$=\left(1-e_0^2\theta^2\nabla^2\right)\left(\frac{\partial^2 w}{\partial x^2}\frac{\partial^2 f}{\partial y^2}-2\frac{\partial^2 w}{\partial x\partial y}\frac{\partial^2 f}{\partial x\partial y}+\frac{\partial^2 w}{\partial y^2}\frac{\partial^2 f}{\partial x^2}+q\right), \tag{17b}$$

$$-D^{**}_{11}\frac{\partial^3 w}{\partial x^3}-\left(D^{**}_{12}+2D^{**}_{66}\right)\frac{\partial^3 w}{\partial x\partial y^2}+G^*_{11}\frac{\partial^2 \psi_x}{\partial x^2}+G^*_{66}\frac{\partial^2 \psi_x}{\partial y^2}+\left(G^*_{12}+G^*_{66}\right)\frac{\partial^2 \psi_y}{\partial x\partial y}-A^*_{44}\psi_x=0, \tag{17c}$$

$$-D^{**}_{22}\frac{\partial^3 w}{\partial y^3}-\left(D^{**}_{12}+2D^{**}_{66}\right)\frac{\partial^3 w}{\partial x^2\partial y}+G^*_{22}\frac{\partial^2 \psi_y}{\partial y^2}+G^*_{66}\frac{\partial^2 \psi_y}{\partial x^2}+\left(G^*_{12}+G^*_{66}\right)\frac{\partial^2 \psi_x}{\partial x\partial y}-A^*_{55}\psi_y=0. \tag{17d}$$

Also, the edge supports at the left and right ends of the microtubule are assumed to be clamped. As a result, one will have: $w=0$, $\frac{\partial w}{\partial x}=0$ at $x=0, L$.

On the other hand, the equilibrium in the x-axis direction can be expressed as

$$\int_0^{2\pi R} N_{xx}\mathrm{d}y + \pi R^2 q = 0. \tag{18}$$

The periodicity condition relevant to a closed shell-type structure reads

$$\int_0^{2\pi R} \frac{\partial v}{\partial y}\mathrm{d}y = 0, \tag{19}$$

which can be rewritten as

$$\int_0^{2\pi R} \left\{ \left(\frac{A_{11}^*}{A_{11}^* A_{22}^* - \left(A_{12}^*\right)^2} \right) \frac{\partial^2 f}{\partial x^2} - \left(\frac{A_{12}^*}{A_{11}^* A_{22}^* - \left(A_{12}^*\right)^2} \right) \frac{\partial^2 f}{\partial y^2} + \frac{w}{R} - \frac{1}{2}\left(\frac{\partial w}{\partial y}\right)^2 + \left(\frac{A_{11}^*}{A_{11}^* A_{22}^* - \left(A_{12}^*\right)^2} \right) N_{yy}^T - \left(\frac{A_{12}^*}{A_{11}^* A_{22}^* - \left(A_{12}^*\right)^2} \right) N_{xx}^T \right\} \mathrm{d}y = 0. \tag{20}$$

Furthermore, the unit end-shortening related to the movable boundary conditions at the left and right ends of the microtubule can be given as

$$\begin{aligned} \frac{\Delta_x}{L} &= -\frac{1}{2\pi RL}\int_0^{2\pi R}\int_0^L \frac{\partial u}{\partial x}\mathrm{d}x\mathrm{d}y \\ &= -\frac{1}{2\pi RL}\int_0^{2\pi R}\int_0^L \left\{ \left(\frac{A_{22}^*}{A_{11}^* A_{22}^* - \left(A_{12}^*\right)^2} \right) \frac{\partial^2 f}{\partial y^2} - \left(\frac{A_{12}^*}{A_{11}^* A_{22}^* - \left(A_{12}^*\right)^2} \right) \frac{\partial^2 f}{\partial x^2} - \frac{1}{2}\left(\frac{\partial w}{\partial x}\right)^2 \right. \\ &\quad \left. + \left(\frac{A_{22}^*}{A_{11}^* A_{22}^* - \left(A_{12}^*\right)^2} \right) N_{xx}^T - \left(\frac{A_{12}^*}{A_{11}^* A_{22}^* - \left(A_{12}^*\right)^2} \right) N_{yy}^T \right\} \mathrm{d}x\mathrm{d}y. \end{aligned} \tag{21}$$

3 Solving process

3.1 Boundary layer theory of nonlocal strain gradient shell buckling

Firstly, the following dimensionless parameters are put to use in order to obtain the asymptotic solutions of the problem in a more general framework:

$$\begin{aligned} &X = \frac{\pi x}{L}, \quad Y = \frac{y}{R}, \quad \beta = \frac{L}{\pi R}, \quad \eta = \frac{L}{\pi h}, \quad \epsilon = \frac{\pi^2 Rh}{L^2}, \\ &\left\{a_{11}^*, a_{22}^*, a_{12}^*, a_{44}^*, a_{55}^*, a_{66}^*\right\} = \left\{ \frac{A_{11}^*}{A_{00}}, \frac{A_{22}^*}{A_{00}}, \frac{A_{12}^*}{A_{00}}, \frac{A_{44}^*}{A_{00}}, \frac{A_{55}^*}{A_{00}}, \frac{A_{66}^*}{A_{00}} \right\}, \\ &\left\{g_{11}^*, g_{22}^*, g_{12}^*, g_{66}^*\right\} = \left\{ \frac{G_{11}*}{A_{00}h^2}, \frac{G_{22}*}{A_{00}h^2}, \frac{G_{12}*}{A_{00}h^2}, \frac{G_{66}*}{A_{00}h^2} \right\}, \\ &\left\{ d_{11}^*, d_{22}^*, d_{12}^*, d_{66}^*, d_{11}^{**}, d_{22}^{**}, d_{12}^{**}, d_{66}^{**} \right\} = \left\{ \frac{D_{11}^*}{A_{00}h^2}, \frac{D_{22}^*}{A_{00}h^2}, \frac{D_{12}^*}{A_{00}h^2}, \frac{D_{66}^*}{A_{00}h^2}, \frac{D_{11}^{**}}{A_{00}h^2}, \frac{D_{22}^{**}}{A_{00}h^2}, \frac{D_{12}^{**}}{A_{00}h^2}, \frac{D_{66}^{**}}{A_{00}h^2} \right\}, \\ &W = \frac{\epsilon w}{h}, \quad F = \frac{\epsilon^2 f}{A_{00}h^2}, \quad \{\Psi_X, \Psi_Y\} = \frac{\epsilon^2 L}{\pi h}\left\{\psi_x, \psi_y\right\}, \\ &\mathcal{P}_q = \frac{3^{3/4} q L R^{3/2}}{4\pi A_{00} h^{3/2}}, \quad \delta_q = \frac{3^{3/4}\Delta_x\sqrt{R}}{4\pi h^{3/2}}, \quad \mathcal{G}_1 = \frac{e_0\theta}{L}, \quad \mathcal{G}_2 = \frac{l}{L}, \end{aligned} \tag{22}$$

in which $A_{00} = E_{22}h$. As a consequence, the nonlinear nonlocal strain gradient governing differential equations can be deduced in boundary layer-type form as

$$\left(\frac{a_{11}^*}{a_{11}^*a_{22}^*-\left(a_{12}^*\right)^2}\right)\frac{\partial^4 F}{\partial X^4}+\left(\frac{1}{a_{66}^*}-\frac{2a_{12}^*}{a_{11}^*a_{22}^*-\left(a_{12}^*\right)^2}\right)\beta^2\frac{\partial^4 F}{\partial X^2\partial Y^2}+\left(\frac{a_{22}^*}{a_{11}^*a_{22}^*-\left(a_{12}^*\right)^2}\right)\beta^4\frac{\partial^4 F}{\partial Y^4}$$
$$+\frac{\partial^2 W}{\partial X^2}=\beta^2\left(\frac{\partial^2 W}{\partial X\partial Y}\right)^2-\beta^2\frac{\partial^2 W}{\partial X^2}\frac{\partial^2 W}{\partial Y^2} \tag{23a}$$
$$\times\left(1-\pi^2\mathcal{G}_2^2\nabla^2\right)\left(\epsilon^2\left(d_{11}^*\frac{\partial^4 W}{\partial X^4}+2\left(d_{12}^*+2d_{66}^*\right)\beta^2\frac{\partial^4 W}{\partial X^2\partial Y^2}+d_{22}^*\beta^4\frac{\partial^4 W}{\partial Y^4}\right)\right.$$
$$-\epsilon\left(d_{11}^{**}\frac{\partial^3\Psi_X}{\partial X^3}+\left(d_{12}^{**}+2d_{66}^{**}\right)\beta\frac{\partial^3\Psi_X}{\partial X^2\partial Y}\right)$$
$$\left.-\epsilon\left(d_{22}^{**}\beta^3\frac{\partial^3\Psi_Y}{\partial Y^3}-\left(d_{12}^{**}+2d_{66}^{**}\right)\beta^2\frac{\partial^3\Psi_Y}{\partial X\partial Y^2}\right)\right)-\frac{\partial^2 F}{\partial X^2}$$
$$\left.+\epsilon^2\left(k_1W-k_2\left(\frac{\partial^2 W}{\partial X^2}+\beta^2\frac{\partial^2 W}{\partial Y^2}\right)\right)\right.$$
$$=\left(1-\pi^2\mathcal{G}_1^2\nabla^2\right)\beta^2\left(\frac{\partial^2 W}{\partial X^2}\frac{\partial^2 F}{\partial Y^2}+2\frac{\partial^2 W}{\partial X\partial Y}\frac{\partial^2 F}{\partial X\partial Y}+\frac{\partial^2 W}{\partial Y^2}\frac{\partial^2 F}{\partial X^2}+\epsilon^{3/2}\frac{4}{3}3^{1/4}\mathcal{P}_q\right) \tag{23b}$$
$$-\epsilon\left(d_{11}^{**}\frac{\partial^3 W}{\partial X^3}+\left(d_{12}^{**}+2d_{66}^{**}\right)\beta^2\frac{\partial^3 W}{\partial X\partial Y^2}\right)+g_{11}^*\frac{\partial^2\Psi_X}{\partial X^2}+g_{66}^*\beta^2\frac{\partial^2\Psi_X}{\partial Y^2}+\left(g_{12}^*+g_{66}^*\right)\beta\frac{\partial^2\Psi_Y}{\partial X\partial Y}$$
$$-a_{44}^*\eta^2\Psi_X=0, \tag{23c}$$
$$-\epsilon\left(d_{11}^{**}\beta^3\frac{\partial^3 W}{\partial Y^3}+\left(d_{12}^{**}+2d_{66}^{**}\right)\beta\frac{\partial^3 W}{\partial X^2\partial Y}\right)+g_{11}^*\beta^2\frac{\partial^2\Psi_Y}{\partial Y^2}+g_{66}^*\frac{\partial^2\Psi_Y}{\partial X^2}+\left(g_{12}^*+g_{66}^*\right)\beta\frac{\partial^2\Psi_X}{\partial X\partial Y}$$
$$-a_{55}^*\eta^2\Psi_Y=0. \tag{23d}$$

The clamped boundary conditions at the left and right ends of the microtubule take the dimensionless form $W=0,\ \frac{\partial W}{\partial X}=0$ at $X=0,\pi$.

Moreover, the dimensionless load–equilibrium relationship along the x-axis takes the following form

$$\frac{1}{2\pi}\int_0^{2\pi}\beta^2\frac{\partial^2 F}{\partial Y^2}\mathrm{d}Y+\frac{2}{3}3^{1/4}\epsilon^{3/2}\mathcal{P}_q=0. \tag{24}$$

In a similar way, the periodicity condition and the unit end-shortening of the microtubule modeled via hyperbolic shear deformation orthotropic shell model can be expresses in dimensionless form, respectively, as follows:

$$\int_0^{2\pi}\left\{\left(\frac{a_{11}^*}{a_{11}^*a_{22}^*-\left(a_{12}^*\right)^2}\right)\frac{\partial^2 F}{\partial X^2}-\left(\frac{a_{12}^*}{a_{11}^*a_{22}^*-\left(a_{12}^*\right)^2}\right)\beta^2\frac{\partial^2 F}{\partial Y^2}+W-\frac{\beta^2}{2}\left(\frac{\partial W}{\partial Y}\right)^2\right.$$
$$\left.+\left(\frac{a_{11}^*\left(a_{22}^*+a_{12}^*\right)}{a_{11}^*a_{22}^*-\left(a_{12}^*\right)^2}\right)\frac{R\alpha_{22}\Delta T}{h}-\left(\frac{a_{12}^*\left(a_{11}^*+a_{12}^*\right)}{a_{11}^*a_{22}^*-\left(a_{12}^*\right)^2}\right)\frac{R\alpha_{11}\Delta T}{h}\right\}\mathrm{d}Y=0 \tag{25}$$
$$\delta_q=-\frac{3^{3/4}}{8\pi^2\epsilon^{3/2}}\int_0^{2\pi}\int_0^{\pi}\left\{\left(\frac{a_{22}^*}{a_{11}^*a_{22}^*-\left(a_{12}^*\right)^2}\right)\beta^2\frac{\partial^2 F}{\partial Y^2}-\left(\frac{a_{12}^*}{a_{11}^*a_{22}^*-\left(a_{12}^*\right)^2}\right)\frac{\partial^2 F}{\partial X^2}-\frac{1}{2}\left(\frac{\partial W}{\partial X}\right)^2\right.$$
$$\left.+\left(\frac{a_{22}^*\left(a_{11}^*+a_{12}^*\right)}{a_{11}^*a_{22}^*-\left(a_{12}^*\right)^2}\right)\frac{R\alpha_{11}\Delta T}{h}-\left(\frac{a_{12}^*\left(a_{22}^*+a_{12}^*\right)}{a_{11}^*a_{22}^*-\left(a_{12}^*\right)^2}\right)\frac{R\alpha_{22}\Delta T}{h}\right\}\mathrm{d}X\mathrm{d}Y. \tag{26}$$

3.2 Perturbation-based solution methodology

As was explained before, the small perturbation parameter ϵ has been utilized to construct the boundary layer-type nonlocal strain gradient governing equation (23). Now, a two-stepped perturbation technique [48–53] is

employed, based on which the independent variables are summarized via the summations of the regular and boundary layer solutions as follows:

$$W = \overline{W}(X, Y, \epsilon) + \widetilde{W}(X, Y, \epsilon, \xi) + \widehat{W}(X, Y, \epsilon, \varsigma), \tag{27a}$$
$$F = \overline{F}(X, Y, \epsilon) + \widetilde{F}(X, Y, \epsilon, \xi) + \widehat{F}(X, Y, \epsilon, \varsigma), \tag{27b}$$
$$\Psi_X = \overline{\Psi}_X(X, Y, \epsilon) + \widetilde{\Psi}_X(X, Y, \epsilon, \xi) + \widehat{\Psi}_X(X, Y, \epsilon, \varsigma), \tag{27c}$$
$$\Psi_Y = \overline{\Psi}_Y(X, Y, \epsilon) + \widetilde{\Psi}_Y(X, Y, \epsilon, \xi) + \widehat{\Psi}_Y(X, Y, \epsilon, \varsigma), \tag{27d}$$

where the accent character $\overline{\ }$ stands for the regular solution, and the accent characters $\widetilde{\ }$ and $\widehat{\ }$ represent the boundary layer solutions in order associated with the left ($X = 0$) and right ($X = \pi$) ends of the microtubule.

Therefore, each part of the solutions can be altered to the perturbation expansions as follows:

$$\begin{aligned}
\overline{W}(X, Y, \epsilon) &= \sum_{i=0} \epsilon^{i/2} \overline{W}_{i/2}(X, Y), \quad \overline{F}(X, Y, \epsilon) = \sum_{i=0} \epsilon^{i/2} \overline{F}_{i/2}(X, Y), \\
\overline{\Psi}_x(X, Y, \epsilon) &= \sum_{i=1} \epsilon^{i/2} \overline{\Psi}_{x_{i/2}}(X, Y), \quad \overline{\Psi}_y(X, Y, \epsilon) = \sum_{i=1} \epsilon^{i/2} \overline{\Psi}_{y_{i/2}}(X, Y), \\
\widetilde{W}(X, Y, \epsilon, \xi) &= \sum_{i=0} \epsilon^{i/2+1} \widetilde{W}_{i/2+1}(X, Y, \xi), \quad \widetilde{F}(X, Y, \epsilon, \xi) = \sum_{i=0} \epsilon^{i/2+2} \widetilde{F}_{i/2+2}(X, Y, \xi), \\
\widetilde{\Psi}_x(X, Y, \epsilon, \xi) &= \sum_{i=0} \epsilon^{i+3/2} \widetilde{\Psi}_{x_{i+3/2}}(X, Y, \xi), \quad \widetilde{\Psi}_y(X, Y, \epsilon, \xi) = \sum_{i=0} \epsilon^{i/2+2} \widetilde{\Psi}_{y_{i/2+2}}(X, Y, \xi), \\
\widetilde{W}(X, Y, \epsilon, \varsigma) &= \sum_{i=0} \epsilon^{i/2+1} \widetilde{W}_{i/2+1}(X, Y, \varsigma), \quad \widehat{F}(X, Y, \epsilon, \varsigma) = \sum_{i=0} \epsilon^{i/2+2} \widehat{F}_{i/2+2}(X, Y, \varsigma), \\
\widehat{\Psi}_x(X, Y, \epsilon, \varsigma) &= \sum_{i=0} \epsilon^{i+3/2} \widehat{\Psi}_{x_{i+3/2}}(X, Y, \varsigma), \quad \widehat{\Psi}_y(X, Y, \epsilon, \varsigma) = \sum_{i=0} \epsilon^{i/2+2} \widehat{\Psi}_{y_{i/2+2}}(X, Y, \varsigma),
\end{aligned} \tag{28}$$

in which ξ and ς denote the boundary layer variables:

$$\xi = \frac{X}{\epsilon^{1/2}}, \quad \varsigma = \frac{\pi - X}{\epsilon^{1/2}}. \tag{29}$$

Afterward, in order to extract the sets of perturbation equations corresponding to both the regular and boundary layer solutions, Eqs. (27) and (28) are inserted in the nonlocal strain gradient governing equation (23) and then the expressions with similar order of ϵ are collected. A tolerance limit < 0.001 is considered to determine the maximum order of ϵ associated with the convergence of the solution methodology.

An initial buckling mode shape for the hyperbolic shear deformable orthotropic shell model under hydrostatic pressure is assumed as

$$\overline{W}_2(X, Y) = \mathcal{A}_{00}^{(2)} + \mathcal{A}_{11}^{(2)} \sin(mX) \sin(nY). \tag{30}$$

Now, some mathematical calculations are carried out to obtain the asymptotic solutions corresponding to each independent variable of the problem which are presented in Appendix A. Subsequently, substitution of them into Eqs. (24) and (26) and then rearranging with respect to the second perturbation parameter ($\mathcal{A}_{11}^{(2)}\epsilon^2$) yields explicit analytical expressions for the nonlocal strain gradient load–deflection and load–shortening stability paths, respectively, as follows:

$$\mathcal{P}_q = \sum_{i=0,2,4,\ldots} \mathcal{P}_q^{(i)} \left(\mathcal{A}_{11}^{(2)}\epsilon^2\right)^i = \mathcal{P}_q^{(0)} + \mathcal{P}_q^{(2)} \left(\mathcal{A}_{11}^{(2)}\epsilon^2\right)^2 + \cdots \tag{31}$$

$$\delta_q = \sum_{i=0,2,4,\ldots} \delta_q^{(i)} \left(\mathcal{A}_{11}^{(2)}\epsilon^2\right)^i - \delta_q^T = \delta_q^{(0)} - \delta_q^T + \delta_q^{(2)} \left(\mathcal{A}_{11}^{(2)}\epsilon^2\right)^2 + \cdots \tag{32}$$

The parameters given in the above equations are introduced in Appendix B. Thereafter, it is supposed that the dimensionless coordinates of the point relevant to the maximum deflection of microtubule are $(X, Y) = (\pi/2m, \pi/2n)$. As a result, one will have

$$\mathcal{A}_{11}^{(2)}\epsilon^2 = \epsilon \frac{w_m}{h} + \mathcal{S}_2 + \mathcal{S}_1 \left(\epsilon \frac{w_m}{h} + \mathcal{S}_2\right)^2, \tag{33}$$

where w_m represents the maximum deflection of hydrostatic pressurized microtubule and the symbols $\mathcal{S}_1$ and $\mathcal{S}_2$ are presented in Appendix B.

4 Numerical results and discussion

Tabulated in Table 1 are the temperature-dependent mechanical properties of a microtubule at different temperatures. Also, in the preceding numerical results, it is supposed that the left and right ends of the microtubule are clamped.

Firstly, in order to check the accuracy of the present solving process, the terms related to the nonlocal strain gradient continuum theory of elasticity are removed and the critical hydrostatic pressures of isotropic cylindrical shells at usual scale (macroscale) are obtained and tabulated in Table 2 corresponding to different geometric parameters, and they are compared with those evaluated by Kasagi and Sridharan [55] using the finite element method. An excellent agreement is found between the two solution methodolgies which confirms the validity of the current solving process.

In Fig. 2, the nonlocal strain gradient load–deflection stability curves of hydrostatic pressurized microtubules are illustrated corresponding to various nonlocal and internal strain gradient length scale parameters. Here, $e_0\theta = 0\,\text{nm}$ or $l = 0\,\text{nm}$ means the classical hyperbolic shear deformable shell model with no size dependency. It can be observed that by increasing the value of the nonlocal parameter, the critical hydrostatic pressure as well as the postbuckling strength of the microtubule reduces, while an increment in the value of the strain gradient parameter increases them. For both types of size effect, a higher value of the small-scale parameter enriches the size dependency in the postbuckling response of the microtubule.

Figure 3 depicts the nonlocal strain gradient load–shortening stability paths of hydrostatic pressurized microtubules in both the prebuckling and postbuckling domains. It is revealed that for a microtubule under hydrostatic pressure, an initial extension occurs in the prebuckling regime until the critical buckling pressure. The nonlocality size effect decreases this initial extension, but the strain gradient size dependency increases it. However, for all cases, the slope of the prebuckling part of the load–shortening stability curve remains constant.

In Figs. 4 and 5, the buckling mode shapes of the hydrostatic pressurized microtubule are demonstrated at a point in the postbuckling regime and in the vicinity of the critical buckling point corresponding to different nonlocal and internal strain gradient length scale parameters, respectively. It is found that the nonlocal size

Table 1 Material properties of a microtubule at different temperatures [30,54]

E_{11} (MPa)	E_{22} (MPa)	$G_{12} = G_{13} = G_{23}$ (MPa)	$\nu_{12} = \nu_{21}$	$\alpha_{11}\left(10^{-6}/^{\circ}\text{C}\right)$	$\alpha_{22}\left(10^{-6}/^{\circ}\text{C}\right)$
$T = 30\,^{\circ}\text{C}$					
127	1.00	1.3	0.3	1.04×10^{-4}	1.04×10^{-4}
$T = 20\,^{\circ}\text{C}$					
138	1.09	1.5	0.3	0.94×10^{-4}	0.94×10^{-4}
$T = 10\,^{\circ}\text{C}$					
178	1.41	1.8	0.3	0.86×10^{-4}	0.86×10^{-4}

Table 2 Comparison of the nonlinear critical buckling pressures (psi) for simply supported isotropic cylindrical shells ($E = 10^7 psi$, $\nu = 0.33$)

$\left(L^2/Rh\right)\sqrt{1-\nu^2}$	Present work	Ref. [55]
$R/h = 50$		
10	1387.44	1390.0
50	559.16	560.0
100	383.29	385.6
500	163.97	165.0
$R/h = 200$		
10	87.06	88.65
50	34.55	35.09
100	23.40	24.26
500	10.02	10.42

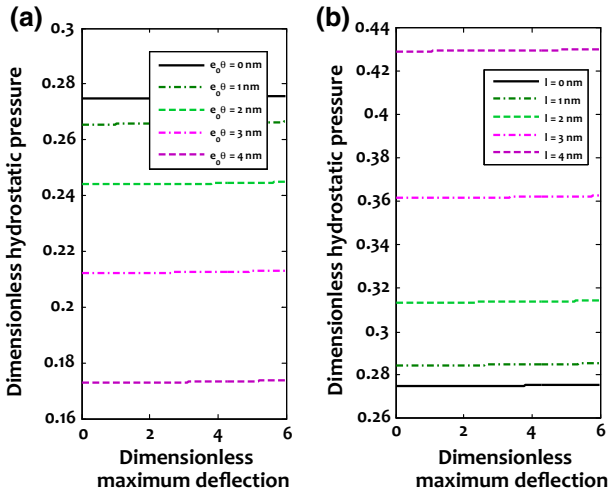

Fig. 2 Dimensionless load–deflection stability paths of microtubule embedded in cytoplasm ($L/R = 10, k_1 = 2.7, k_2 = 0.27, T = 30°\text{C}$); **a** $l = 0\,\text{nm}$, **b** $e_0\theta = 0\,\text{nm}$

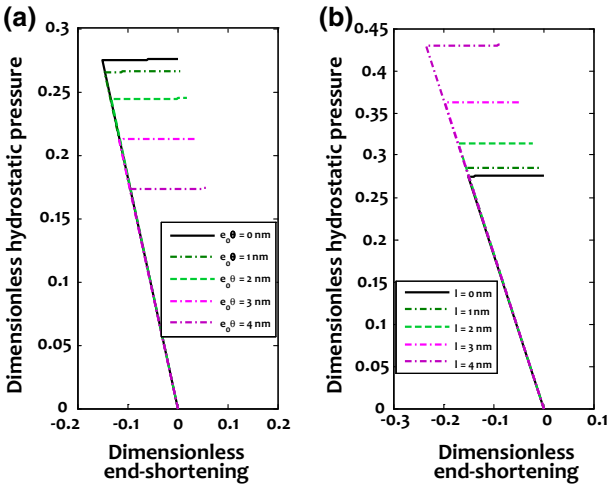

Fig. 3 Dimensionless load–shortening stability paths of microtubule embedded in cytoplasm ($L/R = 10, k_1 = 2.7, k_2 = 0.27, T = 30°\text{C}$); **a** $l = 0\,\text{nm}$, **b** $e_0\theta = 0\,\text{nm}$

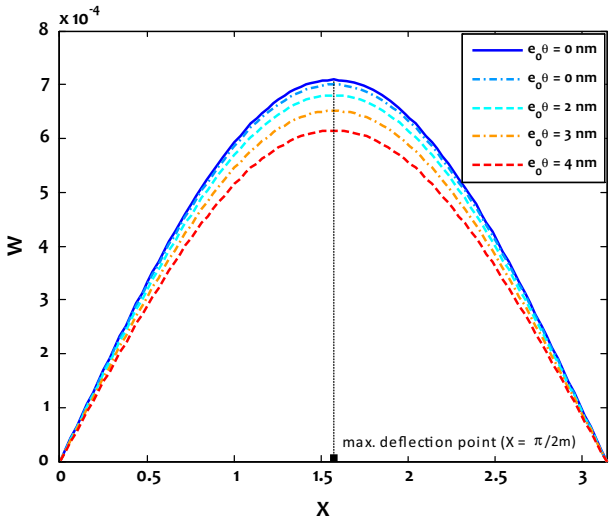

Fig. 4 Dimensionless buckling mode shapes of microtubule embedded in cytoplasm ($L/R = 20, k_1 = 2.7, k_2 = 0.27, l = 0\,\text{nm}$)

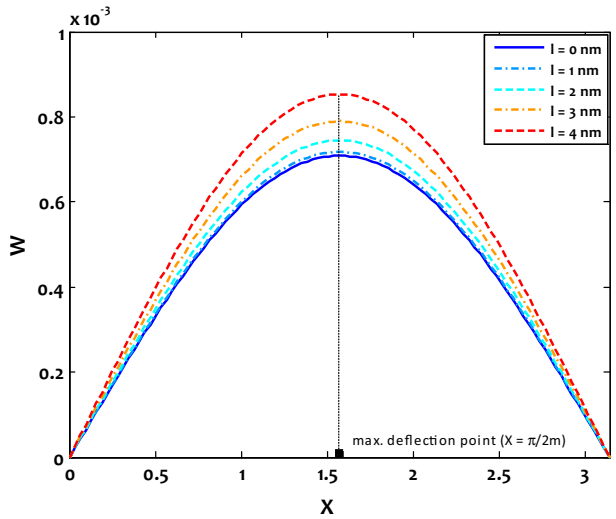

Fig. 5 Dimensionless buckling mode shapes of microtubule embedded in cytoplasm ($L/R = 20, k_1 = 2.7, k_2 = 0.27, e_0\theta = 0$ nm)

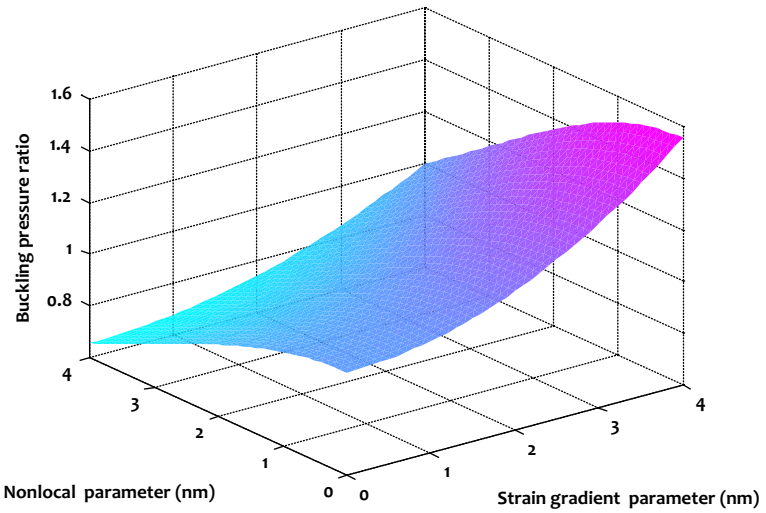

Fig. 6 Variation of the buckling pressure ratio with small-scale parameters

dependency results in a reduction in the maximum deflection of the buckled microtubule, while the strain gradient size effect increases it. Additionally, it has been observed that as has been assumed in the solution methodology, the point at which the maximum deflection of the buckled microtubule occurs has the dimensionless coordinate $X = \pi/2m$, whereas the value of m for a microtubule with $L/R = 20$ is obtained as $m = 1$.

With the aim of answering this question of how much each size dependency affects the critical buckling pressure of a hydrostatic pressurized microtubule, the following buckling pressure ratio is introduced:

$$\text{buckling pressure ratio} = \frac{\text{buckling pressure obtained via local shell model}}{\text{buckling pressure obtained via nonlocal strain gradient shell model}}.$$

The variation of buckling pressure ratio simultaneously with both types of size effect is displayed in Fig. 6. It is seen that by taking $l = 0$ nm and increasing the value of the nonlocal parameter, the buckling pressure ratio reaches its maximum value, while through assuming $e_0\theta = 0$ nm and increasing the value of internal strain gradient length scale parameter, the buckling pressure ratio approaches its minimum value. In addition, there are different combinations of the values of nonlocal and internal strain gradient length scale parameters corresponding to which the buckling pressure ratio remains constant and equal to 1.

Table 3 Dimensionless critical buckling pressures of a hydrostatic pressurized microtubule embedded in cytoplasm biomedium ($L/R = 10, k_1 = 2.7, k_2 = 0.27, T = 30\,^{\circ}\mathrm{C}$)

Small-scale parameter (nm)	Dimensionless buckling load
l = 0	
$e_0\theta = 0$	0.2729
$e_0\theta = 1$	0.2656 (− 3.38%)
$e_0\theta = 2$	0.2440 (− 11.25%)
$e_0\theta = 3$	0.2122 (− 22.80%)
$e_0\theta = 4$	0.1729 (− 37.12%)
$e_0\theta = 0$	
$l = 0$	0.2729
$l = 1$	0.2846 (+ 3.51%)
$l = 2$	0.3136 (+ 14.05%)
$l = 3$	0.3618 (+ 31.62%)
$l = 4$	0.4295 (+ 56.21%)

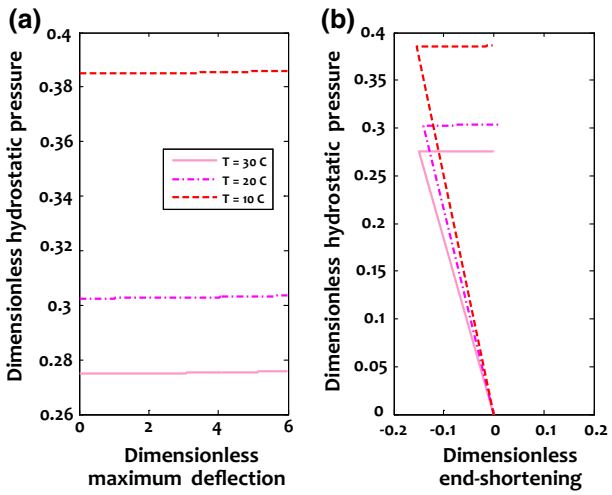

Fig. 7 Influence of temperature change on dimensionless stability paths of microtubule embedded in cytoplasm ($L/R = 10, k_1 = 2.7, k_2 = 0.27, e_0\theta = l = 1$ nm); **a** load–deflection path, **b** load–shortening path

Table 4 Size-dependent critical buckling loads of the microtubule embedded in cytoplasm biomedium corresponding to different temperatures and small-scale parameters ($L/R = 10$)

Temperature	Small-scale parameter (nm)	Critical buckling load
30 °C	$e_0\theta = 0, \quad l = 0$	0.2749
	$e_0\theta = 1, \quad l = 0$	0.2656 (− 3.38%)
	$e_0\theta = 2, \quad l = 0$	0.2440 (− 11.25%)
	$e_0\theta = 3, \quad l = 0$	0.2122 (− 22.80%)
	$e_0\theta = 0, \quad l = 1$	0.2846 (+ 3.51%)
	$e_0\theta = 0, \quad l = 2$	0.3136 (+ 14.05%)
	$e_0\theta = 0, \quad l = 3$	0.3618 (+ 31.62%)
20 °C	$e_0\theta = 0, \quad l = 0$	0.3025
	$e_0\theta = 1, \quad l = 0$	0.2922 (− 3.39%)
	$e_0\theta = 2, \quad l = 0$	0.2653 (− 12.30%)
	$e_0\theta = 3, \quad l = 0$	0.2299 (− 24.00%)
	$e_0\theta = 0, \quad l = 1$	0.3132 (+ 3.53%)
	$e_0\theta = 0, \quad l = 2$	0.3451 (+ 14.08%)
	$e_0\theta = 0, \quad l = 3$	0.3982 (+ 31.64%)
10 °C	$e_0\theta = 0, \quad l = 0$	0.3849
	$e_0\theta = 1, \quad l = 0$	0.3718 (− 3.40%)
	$e_0\theta = 2, \quad l = 0$	0.3375 (− 12.32%)
	$e_0\theta = 3, \quad l = 0$	0.2924 (− 24.03%)
	$e_0\theta = 0, \quad l = 1$	0.3986 (+ 3.55%)
	$e_0\theta = 0, \quad l = 2$	0.4392 (+ 14.11%)
	$e_0\theta = 0, \quad l = 3$	0.5068 (+3 1.68%)

In order to examine the influence of each type of size effect on the critical buckling pressure of the microtubule surrounded by cytoplasm in a living cell, the value of dimensionless critical buckling pressures and the associated relative changes are presented in Table 3 corresponding to various nonlocal and strain gradient parameters. It is indicated that for a specific value of small-scale parameter, the influence of strain gradient size dependency on the critical buckling pressure of the microtubule is more than that of the nonlocal one.

Figure 7 displays the size-dependent load–deflection and load–shortening stability paths of a hydrostatic pressurized microtubule surrounded by the cytoplasm biomedium corresponding to different temperatures. It is indicated that through reduction in temperature, the critical buckling pressure increases. Also, by decreasing the temperature, the negative slope of the prebuckling part of load–shortening stability path reduces.

Also, in Table 4, the dimensionless critical buckling loads of a hydrostatic pressurized microtubule embedded in cytoplasm biomedium are given corresponding to different temperatures and various values of small-scale parameters. It can be observed that by reduction in temperature, both nonlocality and strain gradient size dependency have more influence on the critical buckling load as the associated percent changes increase.

The influence of the cytoplasm biomedium on the load–deflection and load–shortening stability paths of a hydrostatic pressurized microtubule is shown in Figs. 8 and 9, respectively. It is illustrated that by taking the cytoplasm biomedium into consideration, the microtubule buckles at higher hydrostatic pressure. Moreover,

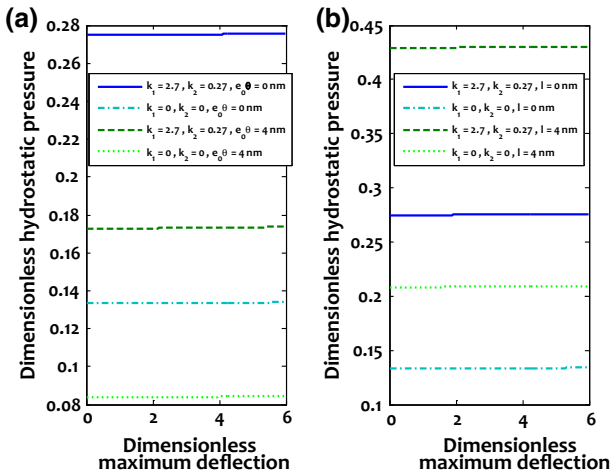

Fig. 8 Influence of the cytoplasm biomedium on dimensionless load–deflection stability paths of microtubule ($L/R = 10$, $T = 30\,^{\circ}\mathrm{C}$); **a** $l = 0$ nm, **b** $e_0\theta = 0$ nm

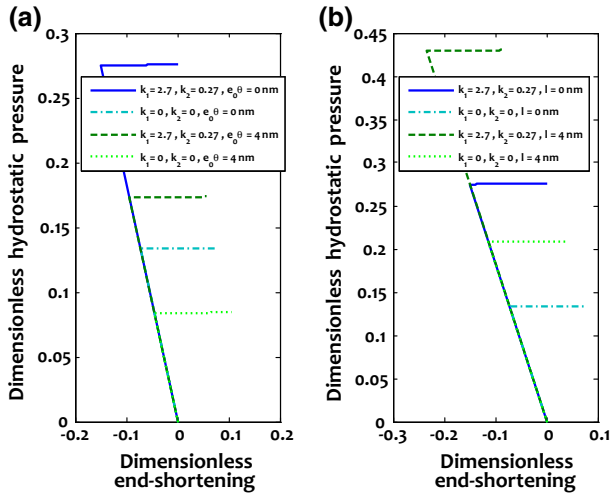

Fig. 9 Influence of the cytoplasm biomedium on dimensionless load–shortening stability paths of microtubule ($L/R = 10$, $T = 30\,^{\circ}\mathrm{C}$); **a** $l = 0$ nm, **b** $e_0\theta = 0$ nm

the cytoplasm biomedium increases the negative shortening associated with the critical point, but it has no influence on the slope of prebuckling part of the load–shortening stability curve.

5 Concluding remarks

The main objective of this study was to examine more comprehensively the size dependency in nonlinear instability characteristics of hydrostatic pressurized microtubules surrounded by the biomedium of cytoplasm in a living cell. To this purpose, nonlocal strain gradient elasticity theory was implemented into a refined hyperbolic shear deformation shell theory to consider jointly the nonlocality and strain gradient microsize dependency. Afterward, boundary layer theory of shell buckling in conjunction with a two-stepped perturbation technique was utilized to achieve explicit analytical expressions for nonlocal strain gradient load–deflection and load–shortening stability curves.

It was found that by increasing the value of nonlocal parameter, the critical hydrostatic pressure as well as the postbuckling strength of microtubule reduces, while an increment in the value of strain gradient parameter increases them. Also, it was revealed that for a specific value of small-scale parameter, the influence of strain gradient size dependency on the critical buckling pressure of the microtubule is stronger than that of the nonlocal one. Moreover, the nonlocality size effect decreases this initial extension, but the strain gradient size dependency increases it. Furthermore, it was displayed that the nonlocal size dependency results in a reduction in the maximum deflection of the buckled microtubule, while the strain gradient size effect increases it. Additionally, it was found that by taking the cytoplasm biomedium into consideration, the microtubule buckles at higher hydrostatic pressure, and the negative shortening associated with the critical point increases.

Acknowledgements The work presented in this paper was supported by a grant from the National Elites Foundation of Iran.

Appendix A

The solutions in asymptotic form corresponding to each of the independent variables are extracted as below:

$$
\begin{aligned}
W = {} & \mathcal{A}_{00}^{(0)} + \epsilon^{3/2}\left[\mathcal{A}_{00}^{(3/2)} - \mathcal{A}_{00}^{(3/2)}\left(\sin\left(\frac{\Gamma_1 X}{\sqrt{\epsilon}}\right) + \cos\left(\frac{\Gamma_1 X}{\sqrt{\epsilon}}\right)\right)e^{-\frac{\Gamma_2 X}{\sqrt{\epsilon}}}\right. \\
& \left. - \mathcal{A}_{00}^{(3/2)}\left(\sin\left(\frac{\Gamma_1 (\pi - X)}{\sqrt{\epsilon}}\right) + \cos\left(\frac{\Gamma_1 (\pi - X)}{\sqrt{\epsilon}}\right)\right)e^{-\frac{\Gamma_2 (\pi - X)}{\sqrt{\epsilon}}}\right] \\
& + \epsilon^2\left[\mathcal{A}_{00}^{(2)} + \mathcal{A}_{11}^{(2)}\sin(mX)\sin(nY) - \mathcal{A}_{00}^{(2)}\left(\sin\left(\frac{\Gamma_1 X}{\sqrt{\epsilon}}\right) + \cos\left(\frac{\Gamma_1 X}{\sqrt{\epsilon}}\right)\right)e^{-\frac{\Gamma_2 X}{\sqrt{\epsilon}}}\right. \\
& \left. - \mathcal{A}_{00}^{(2)}\left(\sin\left(\frac{\Gamma_1 (\pi - X)}{\sqrt{\epsilon}}\right) + \cos\left(\frac{\Gamma_1 (\pi - X)}{\sqrt{\epsilon}}\right)\right)e^{-\frac{\Gamma_2 (\pi - X)}{\sqrt{\epsilon}}}\right] \\
& + \epsilon^3\left[\mathcal{A}_{00}^{(3)} + \mathcal{A}_{11}^{(3)}\sin(mX)\sin(nY)\right] \\
& + \epsilon^4\left[\mathcal{A}_{00}^{(4)} + \mathcal{A}_{11}^{(4)}\sin(mX)\sin(nY) + \mathcal{A}_{20}^{(4)}\cos(2mX) + \mathcal{A}_{02}^{(4)}\cos(2nY)\right] + O\left(\epsilon^5\right) \qquad \text{(A1)} \\
F = {} & -\mathcal{B}_{00}^{(0)}\left(\beta^2 X^2 + \frac{Y^2}{2}\right) + \epsilon\left[-\mathcal{B}_{00}^{(1)}\left(\beta^2 X^2 + \frac{Y^2}{2}\right)\right] \\
& + \epsilon^2\left[-\mathcal{B}_{00}^{(2)}\left(\beta^2 X^2 + \frac{Y^2}{2}\right) + \mathcal{B}_{11}^{(2)}\sin(mX)\sin(nY)\right] \\
& + \epsilon^{5/2}\left[\mathcal{A}_{00}^{\left(\frac{3}{2}\right)}\left(b_{10}^{(2)}\sin\left(\frac{\Gamma_1 X}{\sqrt{\epsilon}}\right) + b_{01}^{(2)}\cos\left(\frac{\Gamma_1 X}{\sqrt{\epsilon}}\right)\right)e^{-\frac{\Gamma_2 X}{\sqrt{\epsilon}}}\right. \\
& \left. + \mathcal{A}_{00}^{(3/2)}\left(b_{10}^{(2)}\sin\left(\frac{\Gamma_1 (\pi - X)}{\sqrt{\epsilon}}\right) + b_{01}^{(2)}\cos\left(\frac{\Gamma_1 (\pi - X)}{\sqrt{\epsilon}}\right)\right)e^{-\frac{\Gamma_2 (\pi - X)}{\sqrt{\epsilon}}}\right] \\
& + \epsilon^3\left[-\mathcal{B}_{00}^{(3)}\left(\beta^2 X^2 + \frac{Y^2}{2}\right) + \mathcal{A}_{00}^{(2)}\left(b_{10}^{(3)}\sin\left(\frac{\Gamma_1 X}{\sqrt{\epsilon}}\right) + b_{01}^{(3)}\cos\left(\frac{\Gamma_1 X}{\sqrt{\epsilon}}\right)\right)e^{-\frac{\Gamma_2 X}{\sqrt{\epsilon}}}\right.
\end{aligned}
$$

$$+\mathcal{A}_{00}^{(2)}\left(\mathcal{b}_{10}^{(3)}\sin\left(\frac{\Gamma_1(\pi-X)}{\sqrt{\epsilon}}\right)+\mathcal{b}_{01}^{(3)}\cos\left(\frac{\Gamma_1(\pi-X)}{\sqrt{\epsilon}}\right)\right)e^{-\frac{\Gamma_2(\pi-X)}{\sqrt{\epsilon}}}\Bigg]$$
$$+\epsilon^4\left[-\mathcal{B}_{00}^{(4)}\left(\beta^2X^2+\frac{Y^2}{2}\right)+\mathcal{B}_{20}^{(4)}\cos(2mX)+\mathcal{B}_{02}^{(4)}\cos(2nY)\right]+O\left(\epsilon^5\right) \tag{A2}$$

$$\Psi_X=\epsilon^2\left[\mathcal{C}_{11}^{(2)}\cos(mX)\sin(nY)+\left(c_{10}^{(2)}\sin\left(\frac{\Gamma_1X}{\sqrt{\epsilon}}\right)+c_{01}^{(2)}\cos\left(\frac{\Gamma_1X}{\sqrt{\epsilon}}\right)\right)e^{-\frac{\Gamma_2X}{\sqrt{\epsilon}}}\right.$$
$$\left.+\left(c_{10}^{(2)}\sin\left(\frac{\Gamma_1(\pi-X)}{\sqrt{\epsilon}}\right)+c_{01}^{(2)}\cos\left(\frac{\Gamma_1(\pi-X)}{\sqrt{\epsilon}}\right)\right)e^{-\frac{\Gamma_2(\pi-X)}{\sqrt{\epsilon}}}\right]$$
$$+\epsilon^3\left[\mathcal{C}_{11}^{(3)}\cos(mX)\sin(nY)\right]+\epsilon^4\left[\mathcal{C}_{11}^{(4)}\cos(mX)\sin(nY)+\mathcal{C}_{20}^{(4)}\sin(2mX)\right]$$
$$+O\left(\epsilon^5\right) \tag{A3}$$

$$\Psi_Y=\epsilon^2\left[\mathcal{D}_{11}^{(2)}\sin(mX)\cos(nY)\right]+\epsilon^3\left[\mathcal{D}_{11}^{(3)}\sin(mX)\cos(nY)\right]$$
$$+\epsilon^4\left[\mathcal{D}_{11}^{(4)}\sin(mX)\cos(nY)+\mathcal{D}_{02}^{(4)}\sin(2nY)\right]+O\left(\epsilon^5\right) \tag{A4}$$

in which

$$\Gamma_1=\sqrt{\frac{\sqrt{\frac{a_{11}^*d_{11}^*}{a_{11}^*a_{22}^*-(a_{12}^*)^2}}}{2}},\qquad \Gamma_2=\sqrt{\frac{\sqrt{\frac{a_{22}^*d_{22}^*}{a_{11}^*a_{22}^*-(a_{12}^*)^2}}}{2}} \tag{A5}$$

Appendix B

$$\mathcal{P}_q^{(0)}=\mathcal{U}_0\mathcal{U}_1\mathcal{U}_8+\mathcal{U}_2\mathcal{U}_8\epsilon^2 \tag{B1}$$

$$\mathcal{P}_q^{(2)}=8\mathcal{U}_1\mathcal{U}_3\mathcal{U}_7\mathcal{U}_8+\frac{8\mathcal{U}_1\mathcal{U}_3\mathcal{U}_8\left(\mathcal{U}_0\mathcal{U}_1\mathcal{U}_6\mathcal{U}_8H_{20}+\mathcal{U}_0\mathcal{U}_3\mathcal{U}_5H_{20}\right)}{\mathcal{U}_0\mathcal{U}_1\mathcal{U}_8H_{20}-\mathcal{U}_5}+\frac{8\mathcal{U}_1\mathcal{U}_3\left(\mathcal{U}_0\mathcal{U}_6+\mathcal{U}_0^2\mathcal{U}_3H_{20}\right)}{\mathcal{U}_0\mathcal{U}_1\mathcal{U}_8H_{20}-\mathcal{U}_5}$$
$$+\frac{8\mathcal{U}_0\mathcal{U}_1\mathcal{U}_3\left(\mathcal{U}_6+\mathcal{U}_0\mathcal{U}_3\right)}{\mathcal{U}_0\mathcal{U}_1\mathcal{U}_8-\mathcal{U}_5}+16\mathcal{U}_0\mathcal{U}_3\mathcal{U}_4\mathcal{U}_8 \tag{B2}$$

$$\delta_q^{(0)}=\left[\frac{\vartheta_1}{2}-\vartheta_2+\left(\frac{\left(2\vartheta_1\vartheta_2-\vartheta_2^2\right)\Gamma_2}{\pi\vartheta_1\left(\Gamma_1^2+\Gamma_2^2\right)}\right)\epsilon^{1/2}\right]\mathcal{P}_q+\left[\left(\frac{3^{1/4}\left(\Gamma_1^2+\Gamma_2^2\right)(2\vartheta_1-\vartheta_2)^2}{6\pi\Gamma_2}\right)\epsilon\right]\mathcal{P}_q^2 \tag{B3}$$

$$\delta_q^{(2)}=\left[\frac{3^{3/4}m^2}{32}\right]\epsilon^{-3/2} \tag{B4}$$

$$\delta_q^{T}=\left(\frac{3^{3/4}}{4}\frac{\alpha_{11}R\Delta T}{h}\right)\epsilon^{1/2} \tag{B5}$$

where

$$H_{11}=1+\pi^2\mathcal{G}_1^2\left(m^2+\beta^2n^2\right)$$
$$H_{20}=1+4\pi^2\mathcal{G}_1^2m^2$$
$$I_{11}=1+\pi^2\mathcal{G}_2^2\left(m^2+\beta^2n^2\right) \tag{B6}$$

where $\mathcal{U}_i$ $(i=0,\ldots,8)$ are constant parameters extracted via the perturbation sets of equations.

$$\mathcal{S}_1=-\left[\left(\frac{2a_{11}^*-a_{12}^*}{a_{11}^*a_{22}^*-\left(a_{12}^*\right)^2}\right)\left(\mathcal{P}_q^{(2)}\right)\right] \tag{B7}$$

$$\mathcal{S}_2=-\left(\frac{2a_{11}^*-a_{12}^*}{a_{11}^*a_{22}^*-\left(a_{12}^*\right)^2}\right)\left(\mathcal{P}_q^{(0)}\right)+\left(\frac{\alpha_{22}R\Delta T}{h}\right)\epsilon \tag{B8}$$

References

1. Venier, P., Maggs, A.C., Carlier, M.F., Pantaloni, D.: Analysis of microtubule rigidity using hydrodynamic flow and thermal fluctuations. J. Biol. Chem. **269**, 13353–13360 (1994)
2. Kurachi, M., Hoshi, M., Tashiro, H.: Buckling of a single microtubule by optical trapping forces—direct measurement of microtubule rigidity. Cell Motil. Cytoskelet. **30**, 221–228 (1995)
3. Fygenson, D.K., Marko, J.F., Libchaber, A.: Mechanics of microtubule-based membrane extension. Phys. Rev. Lett. **79**, 4497–4500 (1997)
4. Odde, D.J., Ma, L., Briggs, A.H., DeMarco, A., Kirschner, M.W.: Microtubule bending and breaking in living fibroblast cells. J. Cell Sci. **112**, 3283–3288 (1999)
5. Yi, D., Wang, T.C., Xiao, Z.: Strain gradient theory based on a new framework of non-local model. Acta Mech. **212**, 51–67 (2010)
6. Fu, Y., Zhang, J., Jiang, Y.: Influences of the surface energies on the nonlinear static and dynamic behaviors of nanobeams. Physica E **42**, 2268–2273 (2010)
7. Akgoz, B., Civalek, O.: Strain gradient elasticity and modified couple stress models for buckling analysis of axially loaded micro-scaled beams. Int. J. Eng. Sci. **49**, 1268–1280 (2011)
8. Wang, B., Zhou, S., Zhao, J., Chen, X.: A size-dependent Kirchhoff micro-plate model based on strain gradient elasticity theory. Eur. J. Mech. A. Solids **30**, 517–524 (2011)
9. Akgoz, B., Civalek, O.: Application of strain gradient elasticity theory for buckling analysis of protein microtubules. Curr. Appl. Phys. **11**, 1133–1138 (2011)
10. Karimi Zeverdejani, M., Tadi Beni, Y.: The nano scale vibration of protein microtubules based on modified strain gradient theory. Curr. Appl. Phys. **13**, 1566–1576 (2013)
11. Demir, C., Civalek, O.: Torsional and longitudinal frequency and wave response of microtubules based on the nonlocal continuum and nonlocal discrete models. Appl. Math. Model. **37**, 9355–9367 (2013)
12. Kiani, K.: Longitudinal, transverse, and torsional vibrations and stabilities of axially moving single-walled carbon nanotubes. Curr. Appl. Phys. **13**, 1651–1660 (2013)
13. Akgoz, B., Civalek, O.: Buckling analysis of linearly tapered micro-columns based on strain gradient elasticity. Struct. Eng.Mech. **48**, 195–205 (2013)
14. Gao, F., Cheng, Q., Luo, J.: Mechanics of nanowire buckling on elastomeric substrates with consideration of surface stress effects. Physica E **64**, 72–77 (2014)
15. Radic, N., Jeremic, D., Trifkovic, S., Milutinovic, M.: Buckling analysis of double-orthotropic nanoplates embedded in Pasternak elastic medium using nonlocal elasticity theory. Compos. B Eng. **61**, 162–171 (2014)
16. Sahmani, S., Bahrami, M., Aghdam, M.M., Ansari, R.: Postbuckling behavior of circular higher-order shear deformable nanoplates including surface energy effects. Appl. Math. Model. **39**, 3678–3689 (2015)
17. Gao, X.-L.: A new Timoshenko beam model incorporating microstructure and surface energy effects. Acta Mech. **226**, 457–474 (2015)
18. Lou, J., He, L., Wu, H., Du, J.: Pre-buckling and buckling analyses of functionally graded microshells under axial and radial loads based on the modified couple stress theory. Compos. Struct. **142**, 226–237 (2016)
19. Akgoz, B., Civalek, O.: Bending analysis of embedded carbon nanotubes resting on an elastic foundation using strain gradient theory. Acta Astronaut. **119**, 1–12 (2016)
20. Kiani, K.: Column buckling of doubly parallel slender nanowires carrying electric current acted upon by a magnetic field. J. Phys. Chem. Solids **95**, 89–97 (2016)
21. Sahmani, S., Aghdam, M.M., Akbarzadeh, A.H.: Size-dependent buckling and postbuckling behavior of piezoelectric cylindrical nanoshells subjected to compression and electrical load. Mater. Des. **105**, 341–351 (2016)
22. Sahmani, S., Fattahi, A.M.: Development an efficient calibrated nonlocal plate model for nonlinear axial instability of zirconia nanosheets using molecular dynamics simulation. J. Mol. Graph. Model. **75**, 20–31 (2017)
23. Sahmani, S., Aghdam, M.M.: Imperfection sensitivity of the size-dependent postbuckling response of pressurized FGM nanoshells in thermal environments. Arch. Civil Mech. Eng. **17**, 623–638 (2017)
24. Sahmani, S., Fattahi, A.M.: Calibration of developed nonlocal anisotropic shear deformable plate model for uniaxial instability of 3D metallic carbon nanosheets using MD simulations. Comput. Methods Appl. Mech. Eng. **322**, 187–207 (2017)
25. Hosseini, M., Dini, A., Eftekhari, M.: Strain gradient effects on the thermoelastic analysis of a functionally graded micro-rotating cylinder using generalized differential quadrature method. Acta Mech. **228**, 1563–1580 (2017)
26. Sahmani, S., Aghdam, M.M., Bahrami, M.: Nonlinear buckling and postbuckling behavior of cylindrical shear deformable nanoshells subjected to radial compression including surface free energy effects. Acta Mech. Solida Sin. **30**, 209–222 (2017)
27. Taghipour, Y., Hosseini, G., Baradaran, H.: Large deflection analysis of nanowires based on nonlocal theory using total Lagrangian finite element method. Acta Mech. **228**, 2429–2442 (2017)
28. Sahmani, S., Aghdam, M.M., Bahrami, M.: Surface free energy effects on the postbuckling behavior of cylindrical shear deformable nanoshells under combined axial and radial compressions. Meccanica **52**, 1329–1352 (2017)
29. Ebrahimi, F., Barati, M.R.: Vibration analysis of viscoelastic inhomogeneous nanobeams resting on a viscoelastic foundation based on nonlocal strain gradient theory incorporating surface and thermal effects. Acta Mech. **228**, 1197–1210 (2017)
30. Shen, H.-S.: Nonlocal shear deformable shell model for postbuckling of axially compressed microtubules embedded in an elastic medium. Biomech. Model. Mechanobiol. **9**, 345–357 (2010)
31. Li, H., Xiong, J.T., Wang, X.: The coupling frequency of bioliquid-filled microtubules considering small scale effects. Eur. J. Mech. A. Solids **39**, 11–16 (2013)
32. Daneshmand, F., Farokhi, H., Amabili, M.: A higher-order mathematical modeling for dynamic behavior of protein microtubule shell structures including shear deformation and small-scale effects. Math. Biosci. **252**, 67–82 (2014)
33. Wang, X., Yang, W.D., Xiong, J.T.: Coupling effects of initial stress and scale characteristics on the dynamic behavior of bioliquid-filled microtubules immersed in cytosol. Physica E **56**, 342–347 (2014)

34. Ghorbanpour Arani, A., Abdollahian, M., Jalaei, M.H.: Vibration of bioliquid-filled microtubules embedded in cytoplasm including surface effects using modified couple stress theory. J. Theor. Biol. **367**, 29–38 (2015)
35. Civalek, O., Demir, C.: A simple mathematical model of microtubules surrounded by an elastic matrix by nonlocal finite element method. Appl. Math. Comput. **289**, 335–352 (2016)
36. Sahmani, S., Aghdam, M.M.: Size-dependent axial instability of microtubules surrounded by cytoplasm of a living cell based on nonlocal strain gradient elasticity theory. J. Theor. Biol. **422**, 59–71 (2017)
37. Lim, C.W., Zhang, G., Reddy, J.N.: A higher-order nonlocal elasticity and strain gradient theory and its applications in wave propagation. J. Mech. Phys. Solids **78**, 298–313 (2015)
38. Li, L., Hu, Y., Li, X.: Longitudinal vibration of size-dependent rods via nonlocal strain gradient theory. Int. J. Mech. Sci. **115–116**, 135–144 (2016)
39. Yang, W.D., Yang, F.P., Wang, X.: Coupling influences of nonlocal stress and strain gradients on dynamic pull-in of functionally graded nanotubes reinforced nano-actuator with damping effects. Sens. Actuators A **248**, 10–21 (2016)
40. Li, L., Hu, Y.: Buckling analysis of size-dependent nonlinear beams based on a nonlocal strain gradient theory. Int. J. Eng. Sci. **97**, 84–94 (2016)
41. Tang, Y., Liu, Y., Zhao, D.: Viscoelastic wave propagation in the viscoelastic single walled carbon nanotubes based on nonlocal strain gradient theory. Physica E **84**, 202–208 (2016)
42. Ebrahimi, F., Barati, M.R.: Hygrothermal effects on vibration characteristics of viscoelastic FG nanobeams based on nonlocal strain gradient theory. Compos. Struct. **159**, 433–444 (2017)
43. Sahmani, S., Aghdam, M.M.: Nonlocal strain gradient beam model for nonlinear vibration of prebuckled and postbuckled multilayer functionally graded GPLRC nanobeams. Compos. Struct. **179**, 77–88 (2017)
44. Li, L., Hu, Y.: Post-buckling analysis of functionally graded nanobeams incorporating nonlocal stress and microstructure-dependent strain gradient effects. Int. J. Mech. Sci. **120**, 159–170 (2017)
45. Zhu, X., Li, L.: Closed form solution for a nonlocal strain gradient rod in tension. Int. J. Eng. Sci. **119**, 16028 (2017)
46. Sawant, M.K., Dahake, A.G.: A new hyperbolic shear deformation theory for analysis of thick beam. Int. J. Innov. Res. Sci. Eng. Technol. **3**, 9636–9643 (2014)
47. Donnell, L.H.: Beam, Plates and Shells, pp. 377–445. McGraw-Hill, New York (1976)
48. Shen, H.-S.: Boundary layer theory for the buckling and postbuckling of an anisotropic laminated cylindrical shell. Part I: Prediction under axial compression. Composite Structures **82**, 346–361 (2008)
49. Shen, H.-S.: Postbuckling of shear deformable FGM cylindrical shells surrounded by an elastic medium. Int. J. Mech. Sci. **51**, 372–383 (2009)
50. Shen, H.-S., Xiang, Y.: Postbuckling of axially compressed nanotube-reinforced composite cylindrical panels resting on elastic foundations in thermal environments. Compos. B Eng. **67**, 50–61 (2014)
51. Sahmani, S., Aghdam, M.M.: A nonlocal strain gradient hyperbolic shear deformable shell model for radial postbuckling analysis of functionally graded multilayer GPLRC nanoshells. Compos. Struct. **178**, 97–109 (2017)
52. Sahmani, S., Aghdam, M.M.: Nonlinear instability of axially loaded functionally graded multilayer graphene platelet-reinforced nanoshells based on nonlocal strain gradient elasticity theory. Int. J. Mech. Sci. **131–132**, 95–106 (2017)
53. Sahmani, S., Fattahi, A.M.: Nonlocal size dependency in nonlinear instability of axially loaded exponential shear deformable FG-CNT reinforced nanoshells under heat conduction. Eur. Phys. J. Plus **132**, 231 (2017)
54. Shi, Y.J., Guo, W.L., Ru, C.Q.: Relevance of Timoshenko-beam model to microtubules of low shear modulus. Physica E **41**, 213–219 (2008)
55. Kasagi, A., Sridharan, S.: Buckling and postbuckling analysis of thick composite cylindrical shells under hydrostatic pressure. Compos. Eng. **3**, 467–487 (1993)